[^{18}F]Fluoroestradiol Radiation Dosimetry in Human PET Studies

David A. Mankoff, Lanell M. Peterson, Timothy J. Tewson, Jeanne M. Link, Julie R. Gralow, Michael M. Graham, and Kenneth A. Krohn

Departments of Radiology and Medical Oncology, University of Washington School of Medicine, Seattle, Washington

[^{18}F]16α-fluoroestradiol (FES) is a PET imaging agent useful for the study of estrogen receptors in breast cancer. We estimated the radiation dosimetry for this tracer using data obtained in patient studies. **Methods:** Time-dependent tissue concentrations of radioactivity were determined from blood samples and PET images in 49 patients (52 studies) after intravenous injection of FES. Radiation absorbed doses were calculated using the procedures of the MIRD committee, taking into account the variation in dose based on the distribution of activities observed in the individual patients. Effective dose equivalent was calculated using International Commission on Radiological Protection Publication 60 weights for the standard woman. **Results:** The effective dose equivalent was 0.022 mSv/MBq (80 mrem/mCi). The organ that received the highest dose was the liver (0.13 mGy/MBq [470 mrad/mCi]), followed by the gallbladder (0.10 mGy/MBq [380 mrad/mCi]) and the urinary bladder (0.05 mGy/MBq [190 mrad/mCi]). **Conclusion:** The organ doses are comparable to those associated with other commonly performed nuclear medicine tests. FES is a useful estrogen receptor-imaging agent, and the potential radiation risks associated with this study are well within accepted limits.

Key Words: PET; estrogen receptor; fluoroestradiol; dosimetry

J Nucl Med 2001; 42:679–684

The compound [^{18}F]16α-fluoroestradiol (FES) is a radioactive tracer used to measure estrogen receptor (ER) expression in tumors and normal tissues (*1–8*). Accurate radiation dosimetry of FES is required to determine the radiation-related risks associated with FES imaging. This article presents estimates of the radiation dose to various organs and to the whole body. The estimates are derived from time–activity curves (TACs) of blood and normal tissue from PET studies of patients with known or suspected breast cancer. They are calculated according to MIRD committee and International Commission on Radiological Protection recommendations (*9–14*).

Received Aug. 3, 2000; revision accepted Dec. 11, 2000.

For correspondence or reprints contact: David A. Mankoff, MD, PhD, Division of Nuclear Medicine, Box 356113, University of Washington School of Medicine, 1959 NE Pacific St., Seattle, WA 98195.

MATERIALS AND METHODS

Subjects

Biodistribution data from 52 FES studies (49 patients), performed at the University of Washington PET Center between January 1996 and June 1999, were used for dosimetry estimates. Because our FES imaging research focused on breast cancer, all patients involved in this study were women (age range, 31–85 y; mean age, 54 y; weight range, 48–110 kg; mean weight, 71 kg). Thirty-three of the patients were postmenopausal. The normal tissues in the imaging data used for dosimetry were distant from the site of any known tumor. The institutional human subjects review committee approved the imaging research protocol, and informed consent was obtained from all patients before imaging.

Radiopharmaceutical

FES was prepared as described previously (*15*). Briefly, ^{18}F is made by the ^{18}O(p,n)^{18}F reaction using $H_2{}^{18}O$ as the target material (*16*). [^{18}F]fluoride anhydrous reacts with 3-methoxymethyl-16β,17β-epiestriol-*O*-cyclic sulfone in refluxing acetonitrile to give [^{18}F]16α-fluoro-17β-sulfate, which is purified by reversed-phase high-performance liquid chromatography (C-18 column eluted with 42% ethanol/water). The sulfate is then hydrolyzed with 0.2N HCl at 140°C to give FES. The specific activity was >30 GBq/μmol (>800 mCi/μmol) in all cases and was typically 37–74 GBq/μmol (1,000–2,000 mCi/μmol).

Data Collection

All patients were positioned supine and imaged using the GE Advance positron emission tomograph (Waukesha, WI). All imaging was performed in a two-dimensional high-sensitivity mode using 35 slices of 4.25-mm thickness on a 15-cm axial field of view. Images were reconstructed with a spatial resolution of 12 mm after correction for scatter and random coincidences. Performance details for the tomograph were reported previously (*17,18*).

Calibration of the PET scanner was performed weekly by imaging vials containing a known quantity of ^{18}F assayed in a dose calibrator (model CRC-12; Capintec, Montvale, NJ). The vial images were reconstructed using the same reconstruction parameters as in the patient studies. This procedure allowed the estimation of tissue TACs in units of MBq/mL from region-of-interest (ROI) analysis of images.

As part of our standard protocol for FES imaging, after a 25-min transmission study, patients were injected with an average of 204 MBq (5.4 mCi) FES (range, 56–296 MBq [1.5–8.0 mCi]) infused over 1–2 min. They underwent dynamic imaging over the area of interest from injection until 60 min after injection. The dynamic imaging sequence was 4 × 20 s, 4 × 40 s, 4 × 1 min, 4 × 3 min, and at 5-min intervals thereafter. The dynamic imaging focused on

the pelvis in four patients and on the thorax/abdominal region in the remaining patients.

To obtain dosimetry information for normal organs, dynamic imaging was interrupted to image the pelvis at approximately 20, 60, and 100 min after injection in 12 patients. In other patients, additional static views were obtained starting at 60 min after injection using 10-min emission scans followed by 15 min of after-injection transmission imaging. Attenuation corrections were applied for each 15-cm field of view that was imaged.

Calculation of Tissue TACs

ROIs were drawn within the boundaries of normal tissue organ volumes determined using transmission images and summed emission images. Blood TACs were obtained from imaged blood-pool activity using 1.9-cm-diameter (16 pixel) ROIs placed in the center of the left ventricle on three adjacent imaging planes (*19*). For red marrow regions, the outline of the spine was visible on summed FES images and used as a guide for ROI placement. ROIs (1.9 cm, 16 pixel) were placed over three adjacent vertebral bodies, and the plane within each vertebral body with the highest uptake was selected. This approach reliably samples the red marrow space and minimizes partial-volume effects. Data from each ROI for each time interval in counts-per-pixel were corrected for image duration and tomograph efficiency using data from the calibration vial. The data were then converted to units of MBq/mL. Lung activity was corrected for tissue density using an assumed value of 0.33 g/mL (*20*). The tissue density in other organs was assumed to be 1.0 g/mL. TACs were normalized to a 37-MBq injection in a 56-kg woman as follows:

$$C'(t) = C(t)\left(\frac{37}{ID}\right)\left(\frac{W}{\bar{W}}\right)\left(\frac{1}{\rho}\right), \qquad \text{Eq. 1}$$

where $C'(t)$ is the corrected TAC (MBq/g) for a 37-MBq injection, $C(t)$ is the TAC from ROI analysis (MBq/mL), ID is the injected dose (MBq), W is the patient weight (kg), $\bar{W}$ is 56 kg, and ρ is the organ density (g/mL). The integrated activity concentration ($\tilde{C}$) for those organs for which fully sampled TACs from 0 to 60 or 90 min were obtained (thoracic and upper abdominal organs) was calculated using trapezoidal integration; extrapolation past the last data point assumed physical decay without biologic clearance. The mean $\tilde{C}$ used in the dosimetry estimates was the average of the individual integrated curves (Bq-h/g).

Additional data were available with more limited temporal resolution for the uterus (10 patients; time range, 12.5–132 min), urinary bladder (16 patients; time range, 12.5–132 min), and intestines (14 patients; time range, 26–118 min). For these organs, $\tilde{C}$ was estimated by combining individual patient data points into a single curve. The decay-corrected pooled data for the urinary bladder and intestines, which come into contact with the tracer largely because of hepatic and urinary clearance, were fit with a rising exponential:

$$C(t) = A(1 - e^{-Bt}), \qquad \text{Eq. 2}$$

TABLE 1
Tissue Uptake of FES for 37-MBq Injection

Organ	No. of studies	$\tilde{C}$ Mean (SD) (kBq-h/g)	Organ mass (g)	$\tilde{A}$ Mean (SD) (MBq-h)
Breast	47	0.7 (0.3)	361	0.2 (0.1)
Gall Bladder	15	31.7 (16.8)	49	1.6 (0.8)
Intestines*				
1	4	5.8 (7.0)		
2	14 (28)	9.8		
3	4 plus pooled	6.6 (6.4)	176 (ULI) + 322 (SmI)	3.3 (3.2)
Blood	48	2.0 (0.5)	347 (heart contents)	0.7 (0.2)
Heart Wall	48	1.8 (0.6)	241	0.4 (0.1)
Kidneys	3	4.2 (0.7)	248	1.0 (0.2)
Liver	49	18.9 (4.8)	1400	26.4 (6.7)
Lungs	48	1.3 (0.5)	651	0.8 (0.3)
Red Marrow	47	1.2 (0.6)	1050	1.2 (0.6)
Spleen	18	1.1 (0.7)	123	0.1 (0.1)
Bladder*				
1	2	14.4 (10.1)		
2	16 (28)	18.3		
3	2 plus pooled	15.7 (7.5)	160	2.5 (1.2)
Uterus*				
1	3	4.8 (2.7)		
2	10 (18)	7.6		
3	3 plus pooled	5.5 (2.6)	79	0.4 (0.2)
Remainder			50,793†	58.9 (7.6)

*These organs also had additional points from more sparsely sampled TACs. 1 = fully sampled curves; 2 = pooled additional data (parentheses indicate number of points used in curve); 3 = mean of fully sampled curves plus additional value from pooled data. These numbers are used for Table 2.

†Remainder of body for 56-kg woman.

ULI = large intestine; SmI = small intestine.

where A and B are arbitrary constants adjusted to fit the measured data.

For the uterus, which has substantial early uptake of FES, decay-corrected data were fit with the following empirically chosen simple γ-variate with two exponentials in the tail (*21*):

$$C(t) = A[te^{-Bt} + (1 - e^{-Ct})(De^{-Et} + Fe^{-Gt})], \quad \text{Eq. 3}$$

where A, B, C, D, E, F, and G are arbitrary constants adjusted to fit the measured data.

The "Solver-Add In" function in EXCEL (Microsoft, Inc., Redmond, WA) was used to minimize the sum of the squares of the differences between the function and the data for each of the tissues. These fits were used simply as a means to fit the curve for integration and were not an attempt to model the kinetics of FES. The fit curves were multiplied by a physical decay factor and then integrated.

The average integrated concentration activity for each organ was obtained from the mean of values from individual patients. For the uterus, bladder, and intestines, the fitted pooled curves from patients with limited time sampling were treated as a single additional value when averaged with the values obtained from patients with full-time sampling of the organ uptake curve.

The total cumulated activity in each organ ($\tilde{A}$) was then calculated by assuming a uniform distribution of activity throughout the organ and multiplying the integrated activity concentration curves (Bq-h/g) by standard reference organ weights for women (*22*).

The remainder of injected activity not accounted for by source organs was assumed to be distributed uniformly in nonsource organ tissues. This assumption is consistent with the uniform uptake seen on FES PET performed outside of source organs and on ER-positive breast tumor sites. Because we assumed no patient voiding after radiotracer injection, the total cumulated activity for a 37 MBq injection is given by the following:

$$A = 37\ \text{MBq} \times \int_0^\infty e^{\frac{-\ln(2)t}{t_{1/2}}} dt, \quad \text{Eq. 4}$$

which is equal to 97.7 MBq-h, where $t_{1/2}$ is the ^{18}F half-life (109.8 min). The cumulated activity in the remainder of the body is therefore given by this number minus the sum of cumulated activities of the source organs. This activity is assumed to be distributed among nonsource tissues for a standard 56-kg woman in proportion to the tissue weights (*22*).

Radiation Dosimetry Calculation

The distribution of absorbed dose was calculated using S values obtained from MIRDOSE3 software (ORISE, Oak Ridge, TN) (*12*) according to the MIRD guidelines (*9–13*). Implicit to the MIRD schema is the assumption that the integrated activity is known for each of the source organs. Observed source organs in this study included the breast, gallbladder, intestines, heart wall, blood, kidney, liver, lung, marrow, spleen, uterus, and bladder. As noted, tissue activity was not significantly different from the image background, defined as soft tissue and muscle uptake, for the other organs, including the ovaries and brain. Therefore, in the MIRD calculation, organs other than source organs were assigned the background level of cumulated activity, calculated as described previously.

Because no S values have been reported for the dose to the lens of the eye, the lens dose was calculated as reported previously (*23*). Static images of the head obtained 60 min or later after injection showed no excessive accumulation of activity in the area of the eye. For all source organs other than the brain, S values for the thyroid were taken as an approximation of lens S values. For the brain, which is in close proximity to the lens, an empirically estimated brain-to-lens S value was used (*23*). Because the brain uptake was at the background level, this estimate had a small effect on the calculated lens dose. The approach to estimating lens dose may slightly overestimate it, because the thyroid is closer than the eye to most of the source organs.

The estimated range of organ doses was calculated assuming gaussian population curves for the integrated source organ activity values, which serve as the input to the MIRD calculations. The SD of the dose to the individual organ was calculated as follows (*24*):

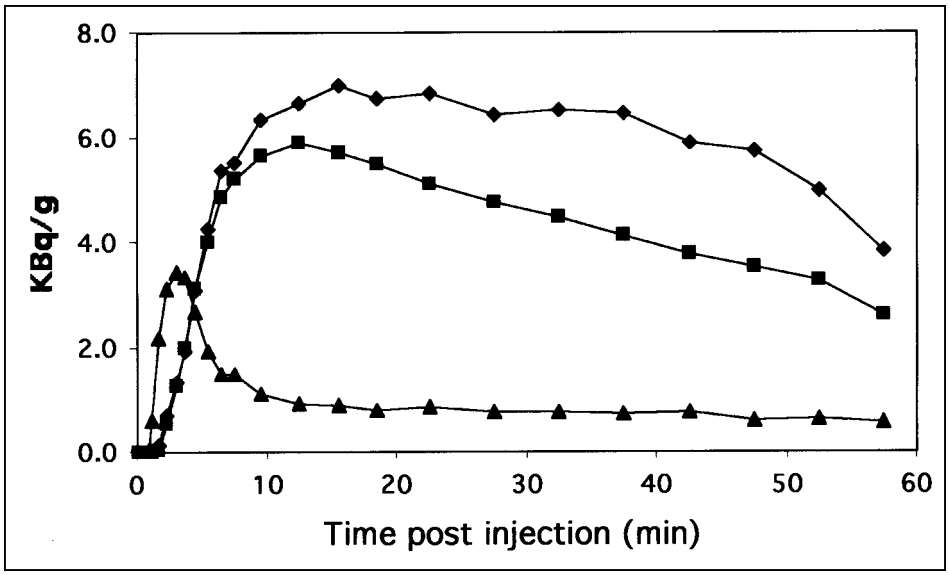

FIGURE 1. Example of TACs for FES in gallbladder (◆), liver (■), and blood (▲). Data are normalized to 37 MBq injected per 56 kg body weight.

$$\sigma_{Di}^2 = \sum_j S_{ij}^2 W_j^2 \sigma_j^2, \qquad \text{Eq. 5}$$

where σ_{Di} is the SD of the estimated dose for the ith organ, σ_j is the SD of the integrated activity for the jth source organ, S_{ij} is the S value for the dose to the ith target organ from the jth source organ, and W_j is the weight of the jth source organ.

Effective Dose Equivalent

The effective dose equivalent for uniform whole-body exposure was calculated using the organ weights of women (*22*), assuming a relative biologic effectiveness of 1.0. The dose estimates for the gonads, bone marrow, colon, lung, stomach, bladder, breasts, liver, esophagus (assumed to be the same as stomach), thyroid, skin, bone surface, and remainder of the body were multiplied by their appropriate weights and summed to calculate the effective dose equivalent.

RESULTS

All the image biodistribution data were normalized for a 37 MBq injection into a 56-kg woman. The integrated activity concentrations ($\tilde{C}$) and cumulated activities ($\tilde{A}$) for the source organs are shown in Table 1. Examples of fully sampled curves are shown in Figure 1. Combined curves and fits for the uterus, intestines, and bladder are shown in Figure 2. For the intestines, activity was visualized only in the small intestines. It was difficult, however, given their anatomic locations, to distinguish between the upper large intestine and small intestine. Therefore, dosimetry was estimated conservatively, assuming identical TACs for both the upper large intestine and the small intestine obtained from ROI analysis of intestinal activity in the PET images. No tracer accumulation was seen in the lower large intestine, sigmoid colon, or rectum, where differentiation from the small bowel is easier.

We did not include data from two men in our dosimetry calculations. The areas under the curves, $\tilde{C}$, for men, normalized to a standard weight of 70 kg for men, fell within the range of values obtained for women (data not shown).

The mean dose, SD, and the 25th and 75th percentiles are given in Table 2. The 25th and 75th percentiles were determined assuming a normal curve with the given mean and SD for each organ. The critical organ was the liver, receiving an average dose of 0.13 mGy/MBq. The effective dose equivalent was 0.022 mSv/MBq.

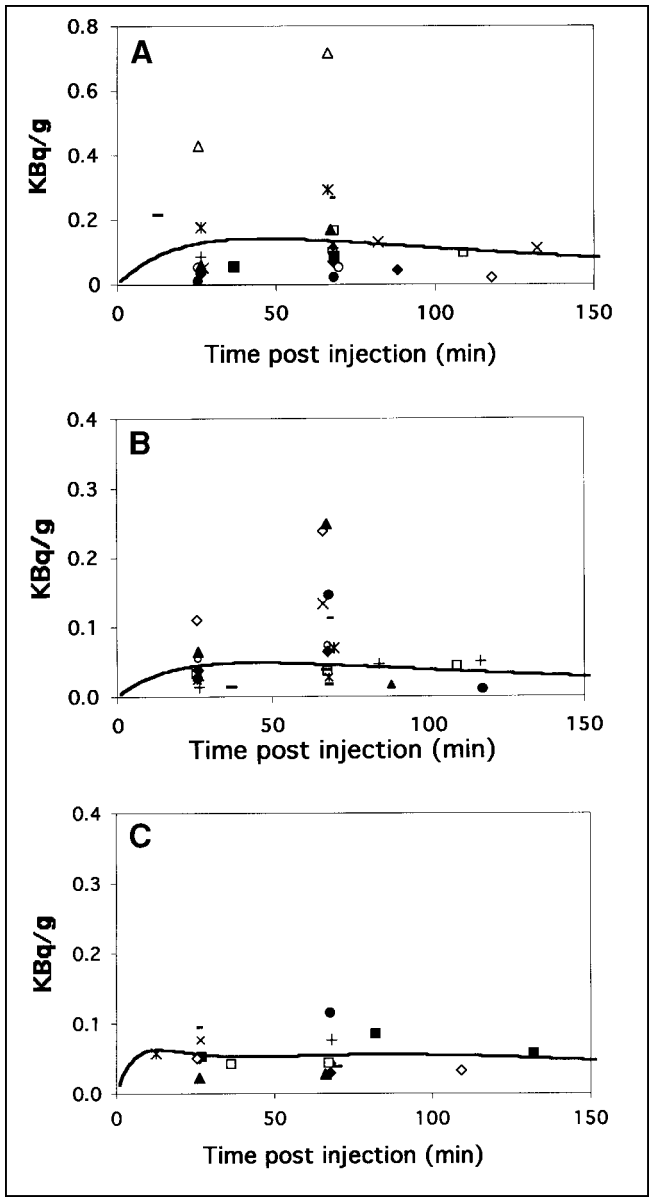

FIGURE 2. FES activity in bladder (A), gastrointestinal tract (B), and uterus (C). Different symbols are used for different studies. Data are normalized to 37 MBq injected per 56 kg body weight. Fits are shown as solid lines. Gastrointestinal tract and bladder data were fit with rising exponential (Eq. 2), and uterus data were fit with function described in Equation 3. *y*-axis for bladder is twice as large as for uterus and intestinal tract.

DISCUSSION

FES shows substantial value as an estrogen receptor imaging agent (*3,4,6,7*). No chemotoxicity from FES was expected, nor has it been noted in our experience. Our investigation therefore concerns only the radiation absorbed dose to better define the radiation risk of FES PET.

In addition to the simplifications inherent in the MIRD phantom model, additional assumptions were made in the analysis of our data. The tracer distribution was assumed to be homogeneous throughout each organ. In addition, tracer clearance occurred by both biologic and physical decay during the course of the imaging study, but clearance was assumed to occur only by physical decay after the final imaging time point. This conservative assumption led to overestimation of the actual radiation exposure. This situation is true especially for the bladder, where voiding was not included in the calculation. Finally, a best-fit curve was used to calculate $\tilde{C}$ from sparsely sampled TACs. This curve fit was chosen on the basis of the observed data. A rising exponential was appropriate for excretory organs (gastrointestinal tract and bladder). An empirically chosen function aided in integrating curves for the uterus.

TABLE 2
Radiation Absorbed Dose to Organs

Organ	Mean* (mGy/MBq)	SD (mGy/MBq)	25%† (mGy/MBq)	75%† (mGy/MBq)
Adrenals	0.023 (85)	0.003	0.021	0.025
Brain	0.010 (36)	0.001	0.009	0.010
Breasts	0.009 (32)	0.002	0.008	0.010
GB wall	0.102 (379)	0.041	0.075	0.134
LLI	0.012 (45)	0.001	0.011	0.013
Small intestine	0.027 (99)	0.015	0.017	0.038
Stomach	0.014 (50)	0.001	0.013	0.014
ULI	0.030 (110)	0.016	0.019	0.042
Heart wall	0.026 (96)	0.004	0.024	0.029
Kidney	0.035 (128)	0.004	0.032	0.038
Liver	0.126 (466)	0.030	0.105	0.149
Lungs	0.017 (61)	0.002	0.015	0.018
Muscle	0.021 (79)	0.001	0.021	0.022
Ovaries	0.018 (66)	0.002	0.016	0.019
Pancreas	0.023 (84)	0.002	0.021	0.024
Red marrow	0.013 (48)	0.002	0.012	0.014
Bone surface	0.014 (53)	0.001	0.014	0.015
Skin	0.005 (18)	0.000	0.005	0.005
Spleen	0.015 (54)	0.003	0.012	0.017
Testes	0.012 (44)	0.001	0.011	0.012
Thymus	0.014 (50)	0.001	0.013	0.014
Thyroid	0.012 (45)	0.001	0.012	0.013
UB wall	0.050 (186)	0.020	0.036	0.066
Uterus	0.039 (145)	0.013	0.031	0.049
Lens	0.009 (33)	0.000	0.009	0.009

*Values in parentheses are mrad/mCi.
†Determined assuming normal curve with given mean and SD.
GB = gallbladder; LLI = lower large intestine; ULI = upper large intestine; UB = urinary bladder.
Effective dose equivalent = 0.022 mSv/MBq (0.004 SD).

The PET acquisition of TACs for FES tissue provides data for the calculation of cumulative radiation doses to each organ that are accurate only within the counting limitations and spatial resolution of the tomograph. Thus, dosimetry calculations of organs smaller than the size that can be visualized, such as the adrenals, were performed assuming average total body concentrations at those sites.

We failed to detect ovary uptake above the background level in 16 patients in whom the ovaries were in the field of view at various times over the course of imaging. Because the ovaries are small, variably positioned, and close to high-uptake organs, such as the uterus and bladder, it is conceivable that ovary uptake slightly above background might not be observed. We therefore calculated ovary dose in a worst-case scenario, for which we assumed the uptake in the ovaries was equal to that in the uterus. In this worst case, the absorbed dose would be 0.036 mGy/MBq (130 mrad/mCi), and an average injected dose of 220 MBq (6 mCi) would still result in an ovary dose <0.010 Gy.

Table 1 shows a larger SD for the integrated TACs for the bladder and uterus in comparison with other organs. The larger variance in the bladder TACs is likely a result of variability in the pattern of FES metabolism and urinary clearance as described previously (*7*), for which we found that the type and quantity of labeled metabolites in the urine could vary significantly between patients. Subjects did not void during the scan. In the uterus, uptake is likely affected by a variety of factors, such as whether or not the patient is postmenopausal, the timing of the scan relative to the menstrual cycle in premenopausal women, and prior hormonal therapy. Our conservative analysis of the variance in dosimetry estimates allows us to estimate the range of bladder and uterine doses that might be encountered, as reflected by the 25th and 75th percentile doses. Even in the worst case, doses for the bladder and uterus are within acceptable limits.

The absence of significant tracer in the lower large intestine is consistent with the known biodistribution and excretion of estradiol (*25*). Estradiol is conjugated and cleared through the biliary system; however, it undergoes substantial enterohepatic circulation. Estradiol excreted through the biliary system and into the small intestines is reabsorbed largely in a conjugated form in the ileum and to a lesser extent in the proximal colon (*25*). Because we could not confidently exclude upper large intestinal activity on the basis of our imaging studies, we conservatively estimated a similar level of activity for the small intestine and upper

large intestine. This assumption does not affect the estimated dose for the critical organ, the liver, as evidenced by the fact that the liver dose has little change if the upper large intestine is not included as a source organ.

CONCLUSION

The organ and total-body doses associated with FES PET imaging are comparable to or lower than those associated with other widely used clinical nuclear medicine procedures (*10*,*13*,*26*,*27*) and are well below the maximum suggested individual study and annual total-body dose of 30 and 50 mGy, respectively, suggested for investigational radiopharmaceuticals by the FDA (*28*). Ongoing clinical trials using FES PET will establish its appropriate role in the study of breast cancer. This analysis indicates that the radiation absorbed dose resulting from the imaging procedure is not a limiting factor and is favorable for further use of this imaging agent. It also suggests that the current recommended maximum dose of approximately 220 MBq (6 mCi) is reasonable for the imaging studies.

ACKNOWLEDGMENTS

The authors thank the PET technologists (Barbara Lewellen, Nancy Bardon, Lisa Dunnwald, Manjeet Basran, Colin Alden, and Pam Pham) for technical assistance, Thomas Lewellen and Steve Kohlmyer for tomograph support, and Svetlana Stekhova for additional radiochemistry support. This study was supported by NIH grants CA42045 and CA72064.

REFERENCES

1. Kiesewetter DO, Kilbourn MR, Landvatter SW, Heiman DF, Katzenellenbogen JA, Welch MJ. Preparation of four fluorine-18-labeled estrogens and their selective uptakes in target tissue of immature rats. *J Nucl Med.* 1984;25:1212–1221.
2. Mathias CJ, Welch MJ, Katzenellenbogen JA, et al. Characterization of the uptake of 16α-([F-18]fluoro)-17β-estradiol in DMBA-induced mammary tumors. *Nucl Med Biol.* 1987;14:15–25.
3. Mintun MA, Welch MJ, Siegel BA, Mathias CJ, Brodack JW, McQuire AH, et al. Breast cancer: PET imaging of estrogen receptors. *Radiology.* 1988;169:45–48.
4. McGuire AH, Dehdashti F, Siegel BA, et al. Positron tomographic assessment of 16α-[F-18]-fluoro-17β-estradiol uptake in metastatic breast carcinoma. *J Nucl Med.* 1991;32:1526–1531.
5. Katzenellenbogen JA, Mathias CJ, Vanbrocklin HF, Welch MJ. Titration of the *in vivo* uptake of 16α-[F-18]fluorestradiol by target tissues in the rat: competition by tamoxifen, and implications for quantitating estrogen receptors *in vivo* and the use of animal models in receptor-binding radioparmaceutical development. *Nucl Med Biol.* 1993;20:735–745.
6. Dehdashti F, Mortimer JE, Siegel BA, et al. Positron tomographic assessment of estrogen receptors in breast cancer: comparison with FDG-PET and *in vitro* receptor assays. *J Nucl Med.* 1995;36:1766–1774.
7. Mankoff DA, Tewson TJ, Eary JF. Analysis of blood clearance and labeled metabolites for the estrogen receptor tracer [F-18]-16α-fluorestradiol (FES). *Nucl Med Biol.* 1997;24:341–348.
8. Moresco RM, Scheithauer BW, Lucignani G, et al. Oestrogen receptors in meningiomas: a correlative PET and immunohistochemical study. *Nucl Med Commun.* 1997;18:606–615.
9. Siegel JA, Thomas SR, Stubbs JB, et al. *Techniques for Quantitative Radiopharmaceutical Biodistribution Data Acquisition and Analysis for Use in Human Radiation Dose Estimates, MIRD Pamphlet No. 16. J Nucl Med.* 1999;40:37S–61S.
10. MIRD. *Radiation Absorbed Dose from Albumin Microspheres Labeled with Tc-99m, MIRD Dose Estimate Report No. 10. J Nucl Med.* 1982;23:915–917.
11. Bouchet LG, Bolch WE, Weber DA, Atkins HL, Poston-Sr JW. *Radionuclide S Values in a Revised Dosimetric Model of the Adult Head and Brain, MIRD Pamphlet No. 15. J Nucl Med.* 1999;40:62S–101S.
12. Stabin MG. MIRDOSE: personal computer software for internal dose assessment in nuclear medicine. *J Nucl Med.* 1996;37:538–546.
13. Stabin MG, Tagesson M, Thomas ST, Ljungberg M, Strand SE. Radiation dosimetry in nuclear medicine. *Appl Radiat Isot.* 1999;50:73–87.
14. International Commission on Radiological Protection. *Recommendations of the International Commission on Radiological Protection.* ICRP Publication 60. Oxford, England: Pergamon Press; 1990.
15. Lim JL, Zheng L, Berridge MS, Tewson TJ. The use of 3-methoxymethyl-16β, 17β-epiestriol-O-cyclic sulfone as the precursor in the synthesis of F-18 16α-fluorestradiol. *Nucl Med Biol.* 1996;23:911–915.
16. Ruth T, Wolf A. Absolute cross sections for the production of ^{18}F via the ^{18}O(p,n) ^{18}F reaction. *Radiochim Acta.* 1979;26:21–25.
17. Lewellen TK, Kohlmyer S, Miyaoka R, Schubert S, Stearns C. Investigation of the count rate performance of the General Electric advance positron emission tomograph. *IEEE Trans Nucl Sci.* 1995;42:1051–1057.
18. DeGrado TR, Turkington TG, Williams JJ, Stearns CW, Hoffman JM, Coleman RE. Performance characteristics of a whole-body PET scanner. *J Nucl Med.* 1994;35:1398–1406.
19. Weinberg IN, Huang SC, Hoffman EJ, et al. Validation of PET-acquired input functions for cardiac studies. *J Nucl Med.* 1988;29:241–247.
20. Rhodes CG, Wollmer P, Fazio F, Jones T. Quantitative measurement of regional extravascular lung density using positron emission and transmission tomography. *J Comput Assist Tomogr.* 1981;5:783–791.
21. Graham MM, Peterson LM, Muzi M, et al. 1-[C-11]Glucose radiation dosimetry and human imaging studies. *J Nucl Med.* 1998;39:1805–1810.
22. Cristy M, Eckerman K. *Specific Absorbed Fractions of Energy at Various Ages from Internal Photon Sources.* ORNL/TM-8381 V1-V7. Oak Ridge, TN: Oak Ridge National Laboratory; 1987.
23. Graham MM, Peterson LM, Link JM, et al. Fluorine-18-fluoromisonidazole radiation dosimetry in imaging studies. *J Nucl Med.* 1997;38:1631–1636.
24. Bevington PR, Robinson DK. *Data Reduction and Error Analysis for the Physical Sciences.* 2nd ed. New York, NY: McGraw-Hill; 1992.
25. Scharl A, Beckmann MW, Artwohl JE, Kullander S, Holt JA. Rapid liver metabolism, urinary and biliary excretion, and enterohepatic circulation of 16α-radioiodo-17β-estradiol. *Int J Radiat Oncol Biol Phys.* 1991;21:1235–1240.
26. Mejia AA, Nakamura T, Masatoshi I, Hatazawa J, Masaki M, Watanuki S. Estimation of absorbed doses in humans due to intravenous administration of fluorine-18-fluorodeoxyglucose in PET studies. *J Nucl Med.* 1991;32:699–706.
27. Wackers FJT, Berman DS, Maddahi J. Technetium-99m hexakis 2-methoxy-isobutyl isonitrile: human biodistribution, dosimetry, safety, and preliminary comparison to thallium-201 for myocardial perfusion imaging. *J Nucl Med.* 1989;30:301–311.
28. Food and Drug Administration. *Food and Drug Administration 21 Code of Federal Regulations.* Pt. 361.1 (b) (3) (i). Washington, DC: Government Printing Office; 2000.